A Novel Architecture Intercalating Redox-Active Polymeric Groups within Graphene Frameworks to Host Platinum Nanoparticles for Methanol Oxidation

Guoyu Shi[1], Zonghua Wang[1,*], Jianfei Xia[1], Jie Tang[2,*], Feifei Zhang[1,2], Yanhui Li[1] , Yanzhi Xia[1] and Linhua Xia[1]

[1]Laboratory of Fiber Materials and Modern Textile, the Growing Base for State Key Laboratory, College of Chemical and Environment Engineering, Qingdao University, Qingdao, Shandong 266071, China;
[2]National Institute for Materials Science, Sengen 1-2-1, Tsukuba 305-0047, Japan
*E-mail: wangzonghua@qdu.edu.cn; Tang.jie@nims.go.jp

Platinum nanoparticles (Pt NPs) are embedded onto poly(acrylic acid)-ferrocene modified graphene nanosheet (PAA-Fc/GN) to form a novel nanocomposite (Pt NPs/PAA-Fc/GN), which is tested for potential use as an anode material through the electrooxidation of methanol. Transmission electron microscope measurements show that Pt NPs evenly disperses onto PAA-Fc/GN with an average particle size of 5.4 nm. Electrochemical measurements demonstrate that Pt NPs/PAA-Fc/GN exhibits higher specific mass activity, enhanced CO-tolerance and superior kinetics for methanol oxidation compared with Pt/GN and traditional PtRu/C catalysts, which is of great significance in direct methanol fuel cell (DMFC) applications. The catalyst's high activity may be attributed to the unique redox-active polymeric frameworks within stacked graphene layers which can not only well accommodate Pt nanoparticles but also provide multidimensional pathways to facilitate the transport of electrons for methanol oxidation.

1. INTRODUCTION

As one of the most promising alternative power sources, direct methanol fuel cell (DMFC) has attracted considerable attention due to its high energy density, low pollutant emission, rich and cheap fuel sources and operation under mild conditions [1-4]. However, commercial applications are hindered by the high cost related to noble metal catalysts and the poisoning caused by intermediate carbonaceous species[5,6,7]. Alloying Pt with other oxophilic elements such as Ru, Ni, Pd, and Au has

been demonstrated rather useful for attenuating CO poisoning and increasing Pt utilization [8-11]. Two main mechanisms are widely accepted to explain this improved tolerance to CO. As to the bifunctional mechanism model [12,13], a second metal can provide oxygenated species at lower potentials for oxidative removal of adsorbed CO. According to the intrinsic or ligand mechanism, the integrated metal modifies the electronic structure of Pt atoms, weakening the bond strength of Pt-CO [14,15]. Although these additional elements enhance the CO-tolerance to a certain extent, their incorporation, mostly with noble metals, makes the DMFC less cost-effective. Thus, new strategy for performance improvement and cost reduction remains the major challenge. The carbon support, which can assist both in dispersing the metal catalyst and in facilitating electron transport, as well as in promoting mass transfer kinetics during the electrochemical reaction, maybe one breakthrough. Graphene nanosheet (GN), a rising star of carbon materials, owning to its high specific surface area and excellent conductivity, has showed wonderful performance as catalyst support for DMFC [16-20]. Recently, some researchers found that the presence of surface functional groups of carbon support can improve wettability and accessibility of methanol to the electro-active surface [21]. These functional groups, of which oxygenated species as the majority, can not only promote the uniform distribution of Pt nanoparticles, but also improve its anti-CO poisoning capability. However, the faint interaction between CO and the oxygenated species because of steric hindrance or the unregulated intervals usually results in sluggish reaction kinetics, which substantially limits the efficiency of DMFC. Therefore, in an effort to reduce anode performance depression induced by CO-poisoning, further decorations on graphene support to endow CO enhanced intimacy or efficient charge transfer with the oxygenated species should be carried out.

Herein, we dressed graphene up by non-covalent functionalization with poly(acrylic acid)-ferrocene (PAA-Fc/GN) and evaluate its performance in loading Pt nanoparticles (Pt-NPs) for fuel cell applications. To our understanding, the allience of PAA-Fc serves not only cross-linking oxygenated anchoring points but also redox-active mediators compared to traditional functional groups, which could accelerate the formation of Pt NPs and the oxidation of CO in terms of uniformity, speed, and energy efficiency. To the best of our knowledge, there is not any report on the application of PAA-Fc/GN as the catalyst support in DMFCs.

Considering the preparation, PAA-Fc can react with graphene oxide (GO) through π-π interaction and analogous hydrophilicity, and then to form oxygenated groups and redox mediators modified GO (PAA-Fc/GO), which can be used as support materials for in situ synthesis of Pt nanoparticles (Pt NPs/PAA-Fc/GN). We found that the presence of PAA-Fc intercalated in GN framework could facilitate the formation of Pt NPs with a smaller size and promote the oxidation of CO. Furthermore, the mechanism on the assistance of PAA-Fc to the enhanced catalytic activity was discussed.

2. MATERIALS AND METHODS

2.1 Preparation of Pt NPs/PAA-Fc/GN catalyst

Reagent grade chemicals were analytical purity otherwise stated. The synthetic route to obtain the PAA-Fc/GN supported Pt NPs (Pt NPs/PAA-Fc/GN) is illustrated in Fig. 1. In our experiment, the

graphene oxide (GO) was prepared according to modified Hummer's method. A solution of PAA-Fc modified graphene oxide (PAA-Fc/GO) was prepared by reacting 2.0 mL of 0.02 M poly (acrylic acid)-ferrocene with 30 mg of GO in 45mL mixed solution ($V_{methanol}$: V_{water} = 1:1) through non-covalent interaction, then the solution was ultrasonicated for 60 min.
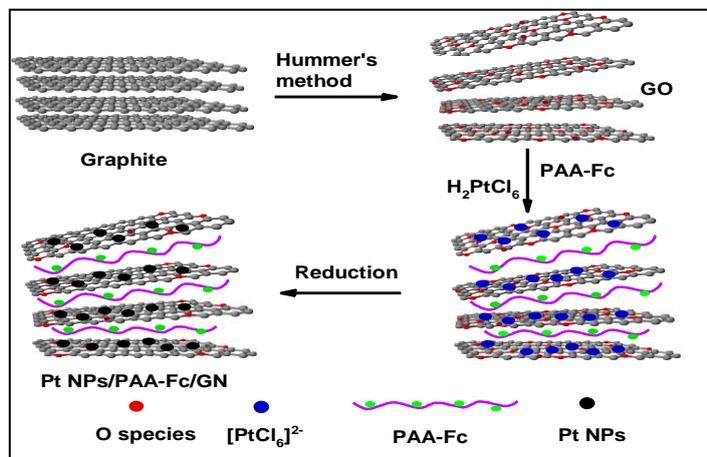

Figure 1. Schematic of the fabrication procedure of Pt NPs/PAA-Fc/GN catalyst.

For the synthesis of Pt NPs, 1mL of 0.038 M H_2PtCl_6 was delivered dropwise into the above solution under vigorous stirring. Subsequently, the pH was appropriately adjusted to a value of 11 by adding a KOH solution (0.5 M) dropwise. Then, 200 mg of $NaBH_4$ was slowly added to the mixture, with stirring for 24 h under room temperature. The black precipitate obtained was filtered, washed several times with methanol-water solution sequentially and collected after drying at 50°C for 24 h in vacuum. For comparison, Pt NPs/GN catalyst was also synthesized following the same procedure without adding PAA-Fc. The Pt content in both samples was 20 wt %.

2.2 Characterization

The morphologies of the synthesized samples were characterized by transmission electron microscopy (TEM) (JEOL, JEM-2100) operating at 200 kV. The bulk composition of the prepared nanocomposites was evaluated by energy dispersive X-ray analysis (EDS) in a scanning electron microscope (JEOL JSM-6700F).

Electrochemical experiments were performed at a CHI-660C electrochemical workstation (Shanghai Chenhua Instrument Co., Ltd.) with a conventional three-electrode cell. A saturated calomel electrode (SCE) and a platinum wire were used as the reference and the counter electrodes, respectively. All the potentials reported in this paper are with respect to this reference electrode. The working electrode was prepared as follows: catalyst powder was ultrasonically dispersed in 0.5% Nafion + C_2H_5OH solution to generate a homogeneous black ink with a content of 1 mg mL^{-1} catalyst. 3 μL of this ink was pipetted onto the glass carbon electrode (3 mm in diameter) and dried using an IR lamp.
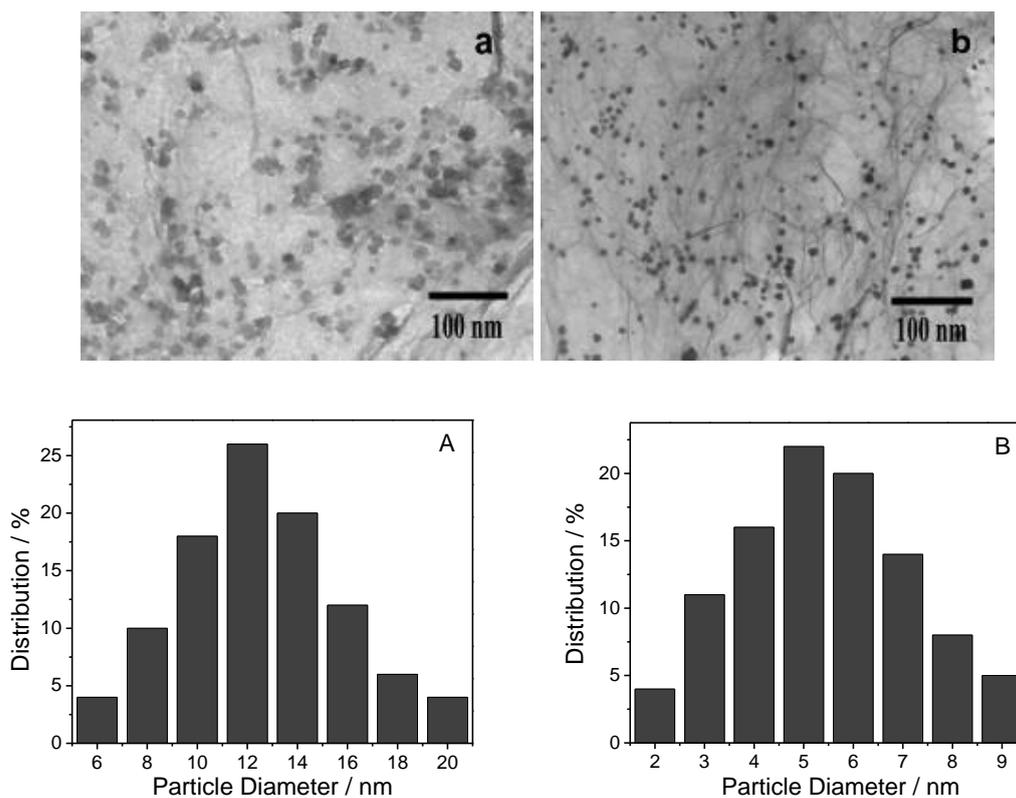
3. RESULTS AND DISCUSSION

Figure 2. TEM images of Pt NPs/GN (a) and Pt NPs/PAA-Fc/GN (b), and the corresponding diameter distribution histograms (A: Pt NPs/GN; B: Pt NPs/PAA-Fc/GN).

TEM images and the corresponding diameter distribution histograms of Pt NPs/GN and Pt NPs/PAA-Fc/GN are shown in Fig. 2. It can be observed that the nanoparticles on PAA-Fc/GN (Fig. 2 b) dispersed much more uniformly and with less aggregation compared to those on GN (Fig. 2 a). Moreover, Pt NPs supported on PAA-Fc/GN (Fig. 2 B) have narrower particle size distribution and smaller average diameter (5.4 nm) compared with that (12.5 nm) of Pt NPs on GN without PAA-Fc (Fig. 2 A), which showed a reasonable agreement with our previous hypothesis that PAA-Fc could facilitate the homogeneous nucleation of Pt NPs with much smaller size through rich anchoring points. In addition, we believe that the graphene sheets were swollen due to the introduction of additional functional groups of hydroxyl, epoxy and carboxyl on the surface of GO after the oxidation reaction. Such a modification is beneficial for hosting PAA-Fc in between the neighboring GN sheets by means of π-π interaction and then additional space was created, which is expected to passivate the GN sheets and prevent their agglomeration. The commodious interspaces and cross-linking architecture within GN frameworks are favorable for buffering ions to shorten the diffusion distances, which leads to more seeding sites and accelerated heterogeneous nucleation for the growth of Pt nanoparticles. Herein, the PAA groups makes a notable difference in dispersion and size for the Pt nanoparticles decorated on the surface of GN: a linker to supply nanoparticles with more sites to deposit and a stabilizer to protect Pt nanoparticles from aggregation and overgrowth.

　　　　The above catalysts were further characterized by EDX. The EDX (Fig. 3) spectra of both catalysts show the peaks corresponding to C, O, Pt elements, of which the elements of C and O are in the majority in GN and PAA-Fc/GN. Moreover, there is a certain amount of Fe (8.20 wt%) for Pt NPs/PAA-Fc/GN (Fig. 3 b), which confirms the existence of Fc on the surface of the graphene nanosheets.
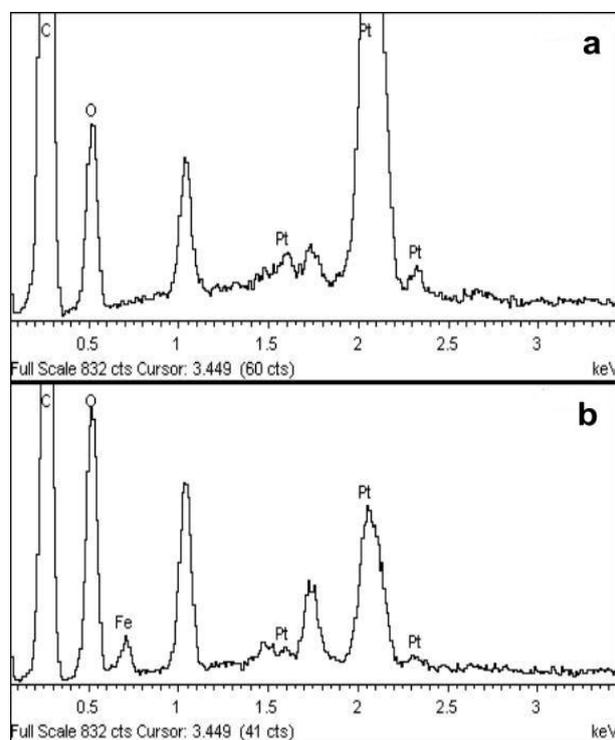

Figure 3. EDX spectra of Pt NPs/GN (a) and Pt NPs/PAA-Fc/GN (b).

　　　　To further prove that Fc was integrated into the composite, the cyclic voltammogram (CV) of the modified electrodes were obtained in PBS (pH 7) (Fig. 4 A). Typically, compared with curve a in Fig. 4 A, a pair of nearly symmetrical redox peaks verifies the integration of Fc in the targeting catalyst Pt NPs/PAA-Fc/GN (Fig. 4 A, curve b).

　　　　The electrochemical activity of the as-prepared catalysts for methanol oxidation reaction was characterized by cyclic voltammetry (CV) and chronoamperometry (CA) measurements in the acidic media. The voltammograms of Pt NPs/GN and Pt NPs/PAA-Fc/GN modified electrodes in 0.5 M H_2SO_4 are shown in Fig. 4 B. All the CV curves exhibited traditional three distinctive potential regions associated with H adsorption/desorption processes ($H^+ + e = H$) between -0.28 and 0.20 V, the double-layer region from 0.20 to 0.40 V, and the formation of an OH_{ad} layer ($2\ H_2O = OH_{ad} + H_3O^+ + e$) beyond 0.4 V. It can be clearly observed that the double-layer capacitance of the Pt NPs/PAA-Fc/GN composite is much larger than that of Pt NPs/GN, indicating the large surface area of PAA-Fc modified graphene nanosheets which renders them the suitable support for the well dispersion of Pt nanoparticles. Moreover, the electrochemically active surface area (ECSA) of Pt NPs was estimated by a calculation of the hydrogen desorption area from the CVs [22]. In this case, the ECSA of Pt

NPs/PAA-Fc/GN is 95.4 m^2 g^{-1}, which is nearly 3 times as large as that of Pt/GN (34.7 m^2 g^{-1}). Hence it can be understood that PAA-Fc plays a vital role in determining the active surface area of graphene support.
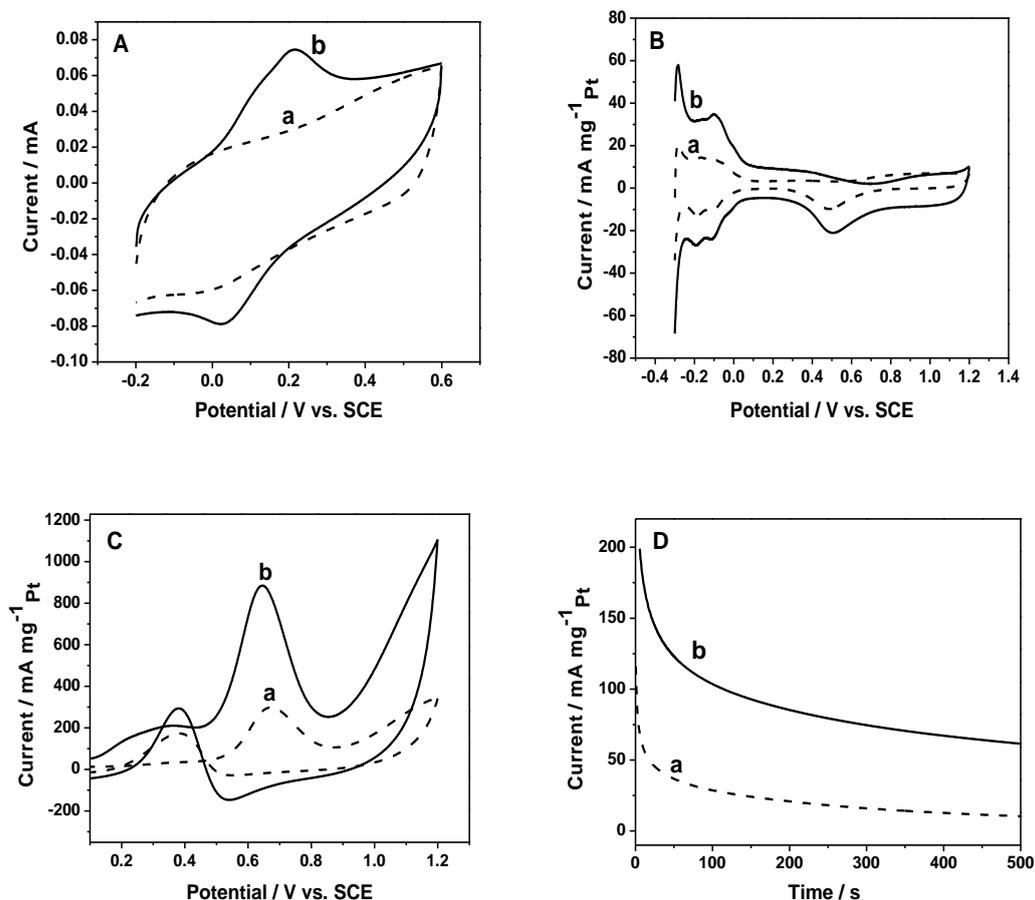

Figure 4. (A) CV curves of Pt NPs/GN (a) and Pt NPs/PAA-Fc/GN (b) in 0.2 M PBS (pH 7.0). (B) CV curves of Pt NPs/GN (a) and Pt NPs/PAA-Fc/GN (b) in 0.5 M H$_2$SO$_4$ aqueous solution. (C) CV curves of the Pt NPs/GN (a) and Pt NPs/PAA-Fc/GN (b) in 0.5 M H$_2$SO$_4$+0.5 M methanol aqueous solution. (D) CA curves of the samples Pt/GN (a) and Pt/PAA-Fc/GN (b) in 0.5 M H$_2$SO$_4$+0.5 M methanol aqueous solution. The scan rate related to the CV is 50 mV s^{-1}. The Pt content in both samples was 20 wt %.

The CVs of the catalysts measured in 1 M H$_2$SO$_4$ + 1 M CH$_3$OH are shown in Fig. 4 C. The oxidation currents have been normalized to mass-specific current density so that the current density can be directly used to compare the activity of the catalysts. From the magnitude of the forward scan peak current (I$_f$), it can be seen that the mass activity of Pt NPs/PAA-Fc/GN (884.2 mA mg^{-1}$_{Pt}$) is considerably higher than that of Pt NPs/GN (298.2 mA mg^{-1}$_{Pt}$), even definitely larger than PtRu/C (717 mA mg^{-1}$_{Pt}$) [23], which is in rational agreement with its higher ECSA value. It also can be seen that the Pt NPs/PAA-Fc/GN catalyst exhibits much more negative onset potential of methanol oxidation than the Pt NPs/GN catalyst. The oxidation peak potential at Pt NPs/PAA-Fc/GN is 0.64 V, about 30 mV more negative than that at Pt NPs/GN (0.67 V), further indicating the easier methanol oxidation reaction on Pt NPs/PAA-Fc/GN. The ratio of forward to backward peak current densities

(I_f/I_b) is generally used to evaluate the poison tolerance of Pt catalysts [24-26]. The observation of ~75% and 150% enhancement on I_f/I_b value of Pt NPs/PAA-Fc/GN (3.02), compared to that of Pt NPs/GN (1.72) and PtRu/C (1.19) [23], indicates a better CO-poisoning tolerance for Pt NPs/PAA-Fc/GN. Thus, it is believed that the cross-linking PAA-Fc structure is a crucial influencing factor for the significant improved electrocatalytic activity.
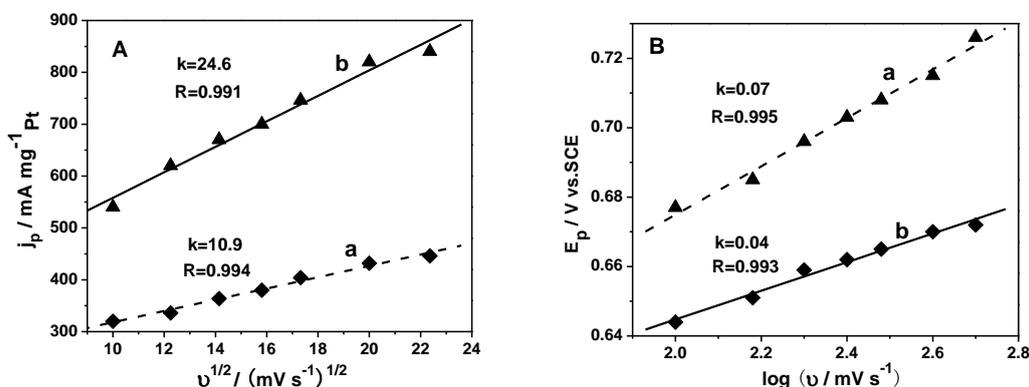

Figure 5. The relationship of peak current density (j_p) vs. the square root of scan rate ($v^{1/2}$) of Pt NPs/GN (a) and Pt NPs/PAA-Fc/GN (b) in 0.5 M H_2SO_4+0.5 M methanol aqueous solution (A), and the corresponding relationship of peak potential (E_p) vs. log (v) (B).
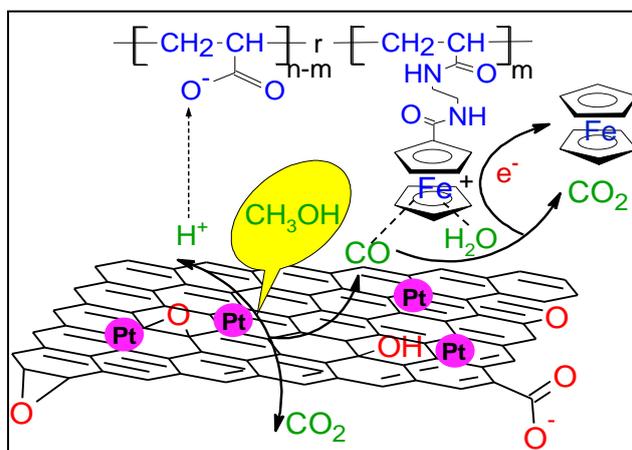

Figure 6. Schematic diagram explaining the high electro-catalytic performance of Pt NPs/PAA-Fc/GN for methanol oxidation.

The stability of the samples was tested by CA and the corresponding results are shown in Fig. 4 D. All catalysts display an initial fast current decay, which is attributed to the formation and accumulation of intermediate species in the oxidation processes, such as CO_{ad} and CHO_{ad}. After a certain period of operation (500 s), although the current continues to decay gradually, the Pt NPs/PAA-Fc/GN electrocatalyst shows a much lower deterioration rate and higher oxidation current compared to the Pt NPs/GN catalyst, demonstrating the prominent electrocatalytic stability of the Pt NPs/PAA-Fc/GN catalyst.

In order to investigate the kinetics of methanol oxidation reaction at Pt NPs/GN and Pt NPs/PAA-Fc/GN electrodes, the relationships between anodic peak current density (I_p) and peak potential (E_p) obtained from forward CV scans with different sweep rates (υ) have also been studied and the plots are shown in Fig. 5. As shown in Fig. 5 A, linear correlation between peak currents and the square roots of the scan rate can be observed from both Pt NPs/GN (a) and Pt NPs/PAA-Fc/GN (b), which signifies obvious diffusion-controlled electrode process[27]. Additionally, the slope of line b (Fig. 5 A, Pt NPs/PAA-Fc/GN) is 24.6 which is about 2.3 times as large as that of line a (Fig. 5 A, Pt NPs/GN, the slope = 10.9). For the diffusion-limited process, the peak current is proportional to the square roots of the scan rate ($\upsilon^{1/2}$) as the followed equation [28]: $i_p = 2.69 \times 10^5 \, n^{3/2} D^{1/2} C \upsilon^{1/2}$. Where D is the diffusion coefficient, C is concentration of the reactant and n represents the number of transfer electrons. Apparently, the slope of the fitted line is dependent on the diffusion coefficient in the equation concerning the peak current and scan rate. Therefore, the larger slope for Pt NPs/PAA-Fc/GN (24.6) compared to Pt NPs/GN (10.9) is indicative of a fast diffusion process of methanol on the surface of PAA-Fc/GN than that on GN supports, which demonstrates that PAA-Fc can effectively improve the kinetics of methanol oxidation.

It also can be seen that the E_p (positive scan) rises with the increase of $\log(\upsilon)$ in Fig. 5 B and shows the linear relationship between E_p and $\log(\upsilon)$, indicating that the oxidation of methanol is an irreversible charge transfer process. Additionally, the linear slope for Pt NPs/PAA-Fc/GN electrode (0.04, line b) is smaller than that for Pt NPs/GN electrode (0.07, line a). In general, the linear relationship of E_p and $\log(\upsilon)$ can be represented with the equation of $k = \dfrac{\partial E_P}{\partial (\lg v)} = 2.3RT / (1-\alpha)nF$ [29,30].

Here, n is given as 6, α stands for the electron transfer coefficient, characterizing the effect of electrochemical potential on the activation energy of an electrochemical reaction. Consequently, the α values are calculated as 0.75 and 0.86 for Pt NPs/PAA-Fc/GN and Pt NPs/GN, respectively. This indicates that Pt NPs/PAA-Fc/GN has smaller activation energy and accordingly enhanced kinetics of methanol electro-oxidation than Pt NPs/GN.

Thus, the PAA-Fc groups interconnected within GN frameworks can significantly enhance the electrocatalytic activity and CO-poisoning tolerance of Pt NP. The possible mechanism is illustrated in Fig.6. For the complete oxidation of methanol to CO_2, a dual path mechanism with the direct pathway going through non-CO_{ad} adsorbates, while the indirect pathway proceeding via the formation of CO_{ad} and its subsequent oxidation, is proposed [31]. Regardless of which pathway, they all experience methanol dissociation and produce hydrogen ions. Herein, the carboxyl anions of PAA can promote the removal of hydrogen ions through electrostatic attraction, which makes the forward oxidation of methanol more inclined. Secondly, the coordinating property of central Fe ion can facilitate the close proximity of abundant oxygenated groups and CO_{ad}, which serves shortcuts or more tendencies for CO oxidation. Furthermore, as a wonderful redox mediator, the Fc group can enhance charge transfer between the carbonaceous species and the catalyst, in addition to the cross-linking and slack architecture of PAA-Fc/GN which accelerates the migrating of CO and other reactants, a faster reaction rate of methanol oxidation can be obtained. The possible mechanism regarding Fc^+ and CO is predicted as follows (1) and (2).

$$Fc^+ + H_2O \rightarrow Fc^+-OH + H^+ + e^- \qquad (1)$$
$$Fc^+-OH + Pt-CO \rightarrow Fc + Pt + CO_2 + H^+ \qquad (2)$$
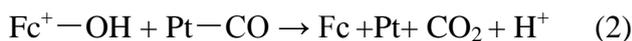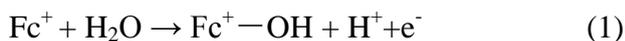
4. CONCLUSION

Our research demonstrates that Pt NPs with uniform small size can be synthesized on the functionalized graphene surface with redox-active polymeric groups. The resulting hybrid Pt NPs/PAA-Fc/GN shows excellent electrocatalytic activity and CO-poisoning tolerance for methanol oxidation, outperforming Pt NPs/GN and commercial PtRu/C electrocatalysts. This new hybrid electrocatalyst can be considered as a promising alternative for improving the efficiency of DMFC and eliminate the use of costly bimetallic or ternary metal systems. In summary, based on the outstanding properties of graphene, nano-decorating of it with various redox-active groups is truly a fascinating route to prepare new support materials for high-performance DMFC.

References

1. K. Darowicki, E. Janicka, P. Slepski, *Int. J. Electrochem. Sci.,* 7 (2012) 12090.
2. H. Wang, S. Ji, W. Wang, V. Linkov, S.r Pasupathi, R. F. Wang, *Int. J. Electrochem. Sci.,* 7 (2012) 3390.
3. J. Masud, M. T. Alama, Z. Awaludin, M. S. El-Deab, T. Okajima, T. Ohsaka, *J. Power Sources* 220 (2012) 399.
4. H. Li, S. C. Zhang, S. H. Yan, Y. Lin, Y. B. Ren, *Int. J. Electrochem. Sci.*, 8 (2013) 2996.
5. H. Wang, S. Ji, W. Wang, V. Linkov, S. Pasupathi, R. F. Wang, *Int. J. Electrochem. Sci.*, 7 (2012) 3390.
6. A. B. Kashyout, A. B. A. A. Nassr, L. Giorgi, T. Maiyalagan, *Int. J. Electrochem. Sci.*, 6 (2011) 379.
7. A. Galal, N. F. Atta, H. K. Hassan, *Int. J. Electrochem. Sci.*, 7 (2012) 768.
8. B. Li, D. C. Higgins, S. M. Zhu, H. Li, H. J. Wang, J. X. Ma, Z. W. Chen, *Catal. Commun* 18 (2012) 51.
9. L. X. Ding, A. L. Wang, G. R. Li, Z. Q. Liu, W. X. Zhao, C. Y. Su, Y. X. Tong, *J. Am. Chem. Soc.* 134 (2012) 5730.
10. H. Q. Ji, M. G. Li, Y. L. Wang, F. Gao, *Electrochem. Commun* 24 (2012) 17.
11. M. Khosravi, M. K. Amini, *Int. J. Hydrogen Energy* 35 (2010) 10527.
12. B. Luo, S. Xu, X. B. Yan, Q. J. Xue, *J. Power Sources* 205 (2012) 239.
13. Y. Y. Feng, L. X. Bi, Z. H. Liu, D. S. Kong, Z. Y. Yu, *J. Catal* 290 (2012) 18.
14. M. T. M. Koper, T. E. Shubina, R. A. Santen, *J. Phys. Chem. B* 106 (2002) 686.
15. M. Wakisaka, S. Mitsui, Y. Hirose, K. Kawashima, *J. Phys. Chem. B* 110 (2006) 23489.

16. S. J. Guo, S. J. Dong, E. K. Wang, *ACS Nano* 4 (2010) 547.
17. Y. M. Li, L. H. Tang, J. H. Li, *Electrochem. Commun.* 11 (2009) 846.
18. J. D. Qiu, G. C. Wang, R. P. Liang, X. H. Xia, H. W. Yu, *J. Phys. Chem. C* 115 (2011) 15639.
19. L. F. Dong, R. Reddy, S. Gari, Z. Li, M. M. Craig, S. F. Hou, *Carbon* 48 (2010) 781.
20. Y. S. Wang, S. Y. Yang, S. M. Li, H. W. Tien, S. T. Hsiao, *Electrochim Acta* 87 (2013) 261.
21. Y. J. Li, W. Gao, L. J. Ci, C. M. Wang, P. M. Ajayan, *Carbon* 48 (2010) 1124.
22. X. D. Xiang, Q. M. Huang, Z. Fu, Y. L. Lin, W. Wu, *Int. J. Hydrogen Energy 37* (2012) 4710.
23. H. Wang, R. F. Wang, H. Li, Q. F. Wang, J. Kang, *Int. J. Hydrogen Energy* 36 (2011) 839.
24. Rajesh, R. K. Paul, A. Mulchandani, *J. Power Sources* 223 (2013) 23.
25. E. Akgül, A. Gülce, H. Gülce, *J. Electroanal. Chem.* 668 (2012) 73.
26. J. G. Hu, B. He, J. Lu, L. J. Hong, J. H. Yuan, J. X. Song, *Int. J. Electrochem. Sci.*, 7 (2012) 10094.
27. H. Tong, H. L. Li, X. G. Zhang, *Carbon* 45 (2007) 2424.
28. Y. Shi, L. Wen, F. Li, H. M. Cheng, *J. Power Sources* 196 (2011).
29. W. C. Ye, H. H. Kou, Q. Z. Liu, J. F. Yan, F. Zhou, C. M. Wang, *Int. J. Hydrogen Energy* 37 (2012) 4088.
30. H. Tang, J. H. Chen, S. Z. Yao, L. H. Nie, *Mater Chem Phys* 92 (2005) 548.
31. T. Iwasita, *Electrochim Acta* 47 (2002) 3663.